Transactions of the Korean Nuclear Society Spring Meeting
Jeju, Korea, May 21-23, 2025

CFD Analysis of Mixing Phenomenon in the OECD/NEA HTGR Lower Plenum Benchmark

Moon Hyeok Kang, Jeong Ik Lee*
Dept. Nuclear & Quantum Eng., KAIST, 291 Daehak-ro, Yuseong-Gu, Daejeon 34141, Republic of Korea
**Corresponding author: jeongiklee@kaist.ac.kr*

Keywords : High Temperature Gas-cooled Reactor, Lower Plenum, Computational Fluid Dynamics

1. Introduction

One of the promising future reactor concepts, High Temperature Gas-cooled Reactor (HTGR), is under the conceptual development in Korean. The HTGR employs a prismatic core configuration and uses helium as the working fluid. As helium flows through the reactor core to remove the heat generated in the prismatic fuel columns, it then converges in the lower plenum. Because of significant radial temperature gradients in the incoming helium streams, complex thermal mixing occurs in the lower plenum before the fluid exits via the outlet (hot duct). The flow pattern in the lower plenum is highly turbulent and involves heat transfer around multiple support structures, making it difficult to measure experimentally.

To address these challenges, the OECD/NEA has initiated a benchmark study on HTGR lower plenum mixing in collaboration with several international institutions [1]. Experimental data are obtained from Oregon State University's High Temperature Test Facility (HTTF), which closely resembles the HTGR's reference model. These benchmark results provide valuable insight into the design of a domestic HTGR by confirming the accuracy of computational predictions.

These benchmarking activities can significantly contribute to the conceptual design of the domestic HTGR. Before conducting the HTGR experimental research, the preliminary design must be conceptualized and analyzed. For this purpose, thermodynamic state variables of the primary system will be obtained at various locations and can be derived through numerical calculations with a Computational Fluid Dynamics (CFD) code or a system analysis code.

In the preliminary design of an HTGR, thermodynamic variables throughout the primary system (including the lower plenum) must be evaluated. Such evaluations often rely on numerical methods such as CFD or system analysis codes. To increase confidence in these predictions, thorough verification and validation against high-quality experimental data and widely accepted benchmark problems are required. According to Oberkampf [2], the reliability of a simulation improves with the independence and rigor of its verification activities. Hence, comparisons and the use of different CFD programs, numerical schemes, and meshing strategies are strongly encouraged.

Considering these points, this paper presents CFD simulation results from KAIST for the OECD/NEA Lower Plenum Benchmark study. Although the final benchmark report is scheduled for release in December 2025, this paper focuses on the preliminary simulation outcomes that highlight the mixing phenomenon in the HTGR lower plenum.

2. Methodology

The three-dimensional lower plenum geometry was provided to benchmark participants by the OECD/NEA organizers [3]. Fig. 1 depicts the overall geometry with red inlet ducts and a blue hot duct. Fig. 2 shows the graphite support posts that promote flow mixing within the plenum.

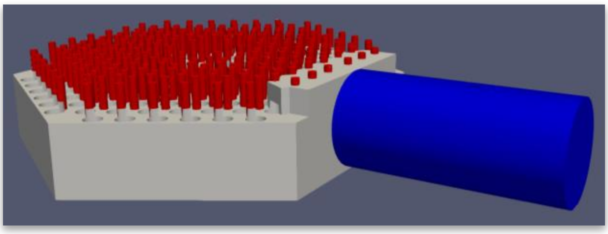

Fig. 1. Schematic view of HTGR lower plenum geometry

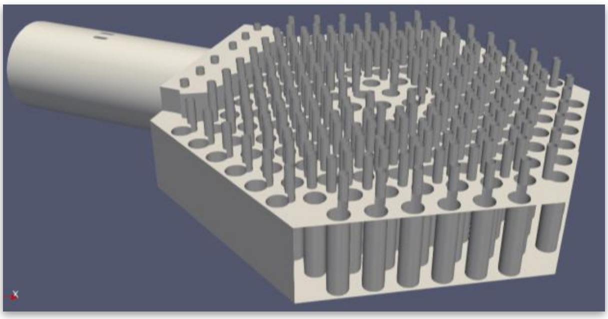

Fig. 2. Graphite support posts inside the plenum

Meshing was conducted using OpenFOAM v2406's snappyHexMesh. To check mesh sensitivity, the domain was divided into three different mesh densities—coarse, medium, and fine. Table 1 summarizes the mesh details. The characteristic cell size, *h*, was calculated by Eq. 1.

$$h = \left(\frac{domain\ volume}{cell\ number}\right)^{1/3} \quad (1)$$

The near-wall cells were refined such that the average y^+ value remained within the viscous sublayer ($y^+ < 5$), allowing a low-Reynolds number approach near the walls.

Table 1. Detailed mesh information

	Coarse	Medium	Fine
Cells (#)	17.4M	26.4M	43.8M
Characteristic cell size (mm)	2.36	2.06	1.74
Average y+	2.78	2.24	1.75

Fig. 3 show snapshots of the mesh, highlighting refinements near the support posts and within the hot duct entrance to accurately capture the rapid velocity increase at the hot duct entrance.

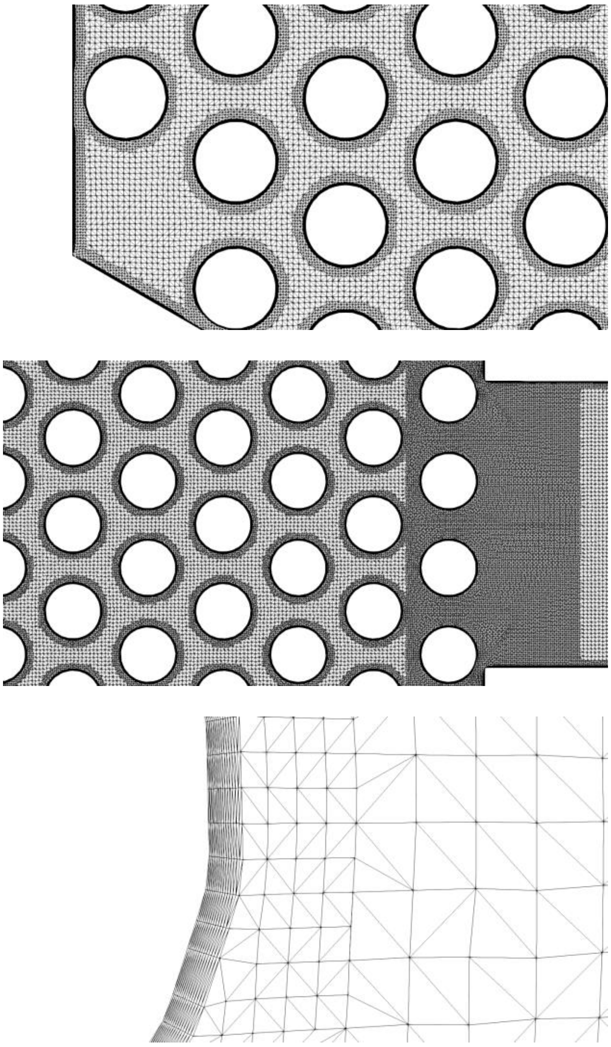

Fig. 3. Snapshots of the internal mesh

The boundary conditions are set as follows :

Wall Boundaries: Adiabatic and no-slip conditions were imposed on all plenum walls.

Inlets: Mass flow rates and temperatures were specified for each inlet duct. Inlet ducts are grouped into channel groups (CG), each with a distinct temperature and flow rate (see Appendix for details).

Outlet: The outlet was prescribed with a constant pressure boundary. For all other variables (e.g., temperature, velocity), zero-gradient conditions were applied in the axial direction of the hot duct.

The CFD solver buoyantSimpleFoam in OpenFOAM v2406 was used for steady-state compressible turbulent flow. A standard k-ε turbulence model was selected. Given the negligible pressure drop across the lower plenum [3], helium was assumed to behave as a calorically perfect gas with temperature-dependent properties [1].

3. Mesh Sensitivity Study of CFD Simulations

A mesh sensitivity study was performed by comparing velocity magnitude and temperature profiles along the centerlines of the lower plenum and hot duct for the three mesh cases. Fig. 4 and 5 illustrate the velocity and temperature profiles along the lower plenum centerline, whereas Fig 6 and 7 show corresponding profiles along the hot duct centerline. In all cases, the computed mass imbalance was approximately 0.1158%, indicating minimal numerical error and negligible stagnation. The profiles across different mesh resolutions were asymptotically similar.

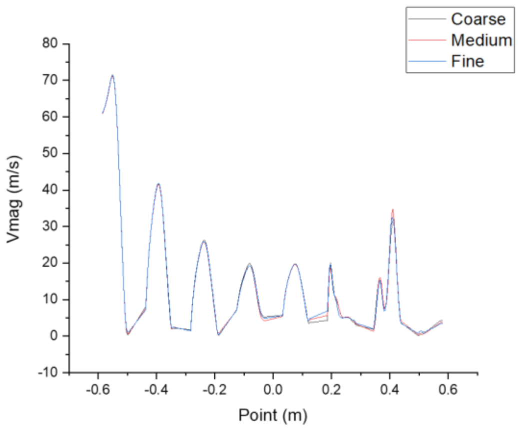

Fig. 4. Velocity magnitude at the centerline of the lower plenum

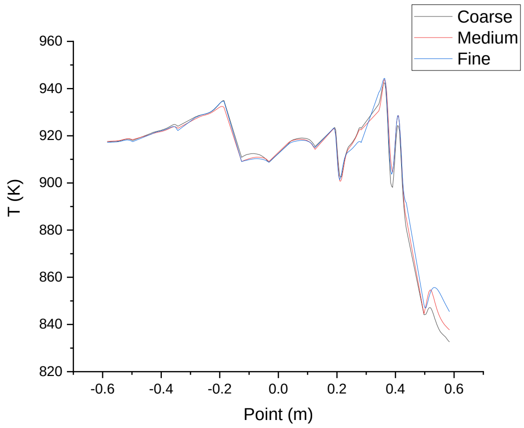

Fig. 5. Temperature at the centerline of the lower plenum

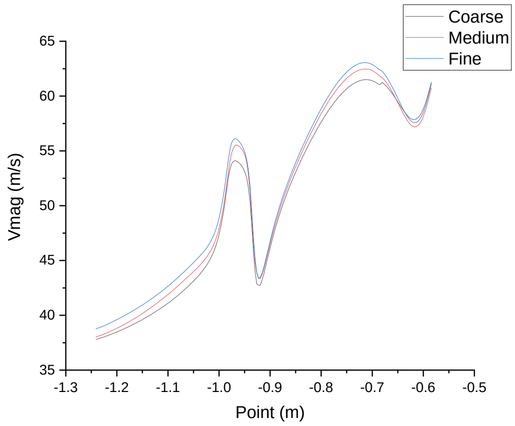

Fig. 6. Velocity magnitude at the centerline of the hot duct

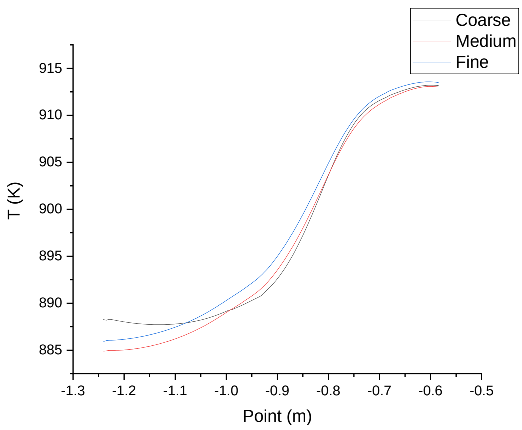

Fig. 7. Temperature at the centerline of the hot duct

4. Results and Discussions

Fig 8 and 9 present streamline plots colored by temperature and velocity magnitude, respectively. A sharp increase in velocity is observed where the flow converges into the hot duct.

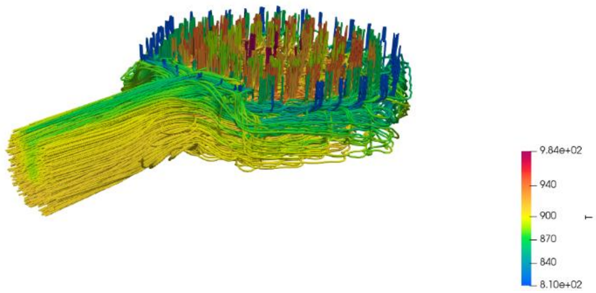

Fig. 8. Temperature streamlines near hot duct

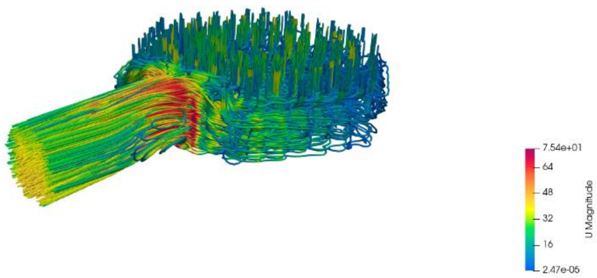

Fig. 9. Velocity magnitude streamlines near hot duct

To analyze local mixing patterns, Figures 10 and 11 show the velocity magnitude and temperature distributions on a horizontal plane at 25% of the lower plenum's height. Due to the presence of numerous support posts, the velocity remains relatively low within the plenum, and the fluid cools as it mixes with surrounding streams. Several local hot spots appear near inlet ducts carrying high-temperature helium (>980 K). These spots dissipate quickly, as shown in Fig 12 and 13, through mixing with cooler streams.

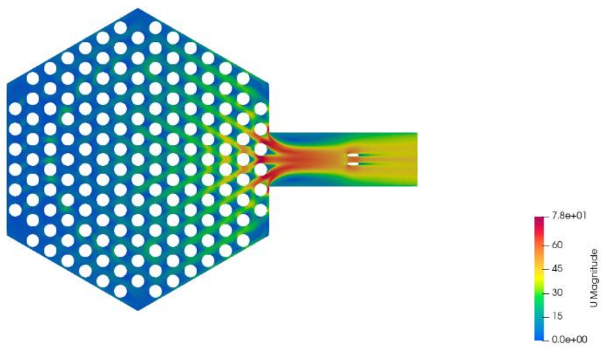

Fig. 10. Velocity magnitude horizontal plane 25% LP

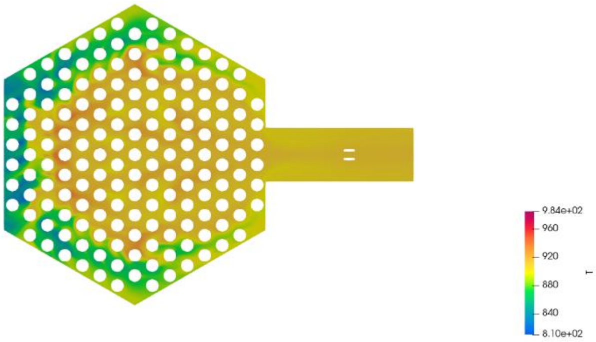

Fig. 11. Temperature horizontal plane 25% LP

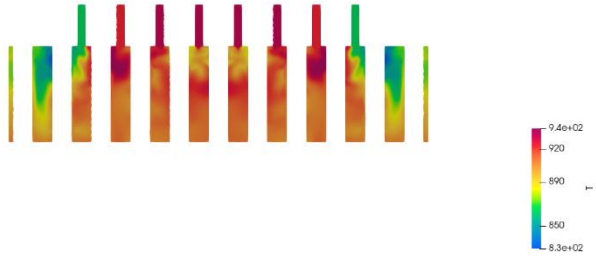

Fig. 12. Temperature plane at the center of the lower plenum (vertical axis to hot duct)

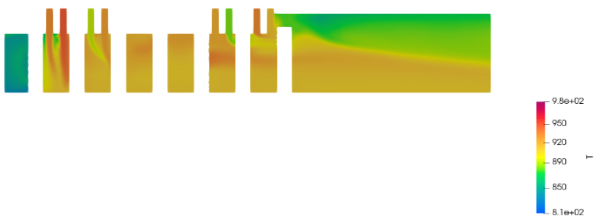

Fig. 13. Temperature plane at the center of the lower plenum (horizontal axis to hot duct)

To visualize the hottest fluid regions, Fig 14 highlights areas where $|T - T_{max}| < 5K$. Fig 15 offers a three-dimensional temperature field within the lower plenum. Overall, most high-temperature regions remain localized near specific inlet ducts and the adjacent support posts. The bulk flow temperature is relatively uniform with significant differences of radial inlet temperatures, which is a result of continuous mixing.

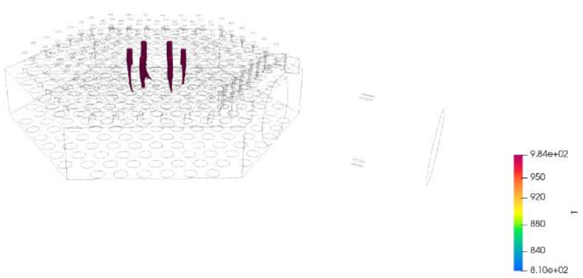

Fig. 14. Temperature distribution for $|T - T_{max}| < 5K$

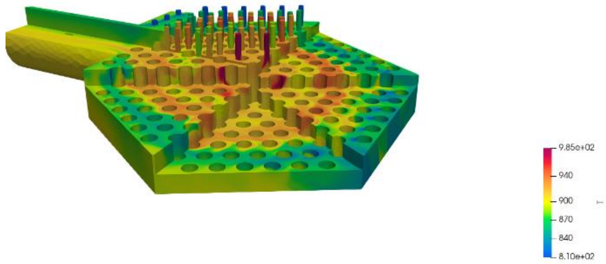

Fig. 15. Temperature plot inside the lower plenum

5. Summary and Conclusions

In this study, CFD simulations were performed as part of the OECD/NEA HTGR Lower Plenum Benchmark to investigate thermal mixing in the lower plenum. The steady-state compressible solver in OpenFOAM v2406 was used with a standard k-ε turbulence model. The following conclusions can be drawn:

Mixing Behavior: Strong mixing was observed in the lower plenum, resulting in relatively uniform temperatures except for a few localized hot spots near high-temperature inlet ducts.

Mesh Sensitivity: A mesh independence study showed that solutions converged with minimal mass imbalance and negligible stagnation zones.

Flow Characterization: High-velocity streams were primarily confined to the inlet ducts and the hot duct. Support posts distributed within the plenum effectively reduced the velocity magnitude and promoted heat transfer.

Future Work: The final benchmark comparisons with experimental data from the HTTF will help validate the numerical modeling strategies. These results will be included in the official benchmark report scheduled for release in December 2025.

Overall, the preliminary CFD results indicate that the lower plenum design effectively mitigates large temperature gradients and maintains a uniform outlet temperature. Ongoing efforts will focus on further validation, transient analyses, and exploring potential design optimizations for advanced HTGR systems.

ACKNOWLEDGEMENT

This work was supported by the National Research Foundation of Korea(NRF) grant funded by the Korea government (MSIT) (No. RS-2024-00457356).

The authors thank Aaron Epiney and Izabela Gutowska for coordinating the benchmark and providing the necessary materials.

Reference

[1] Hua, Thanh, Jun Fang, and Ling Zou. HTTF Benchmarking Activities in FY 2023. No. ANL/NSE-23/55. Argonne National Laboratory (ANL), Argonne, IL (United States), 2023.

[2] Oberkampf, William L., and Christopher J. Roy. Verification and validation in scientific computing. Cambridge university press, 2010.

[3] Halsted, Joshua, and Izabela Gutowska. "Verification and validation of a lower plenum mixing test at the OSU High Temperature Test Facility." Nuclear Engineering and Design 406 (2023): 112251.

APPENDIX

Zone ID	Velocity (m/s)	Temperature (K)
CG0	**30.389**	**984.34**
CG-1A	**23.513**	**924.658**
CG-2A	**25.709**	**889.08**
CG-3A	**26.618**	**944.901**
CG-4A	**26.405**	**926.654**
CG-5A	**21.83**	**866.424**
CG-1B	**23.513**	**925.415**
CG-2B	**25.69**	**890.425**
CG-3B	**26.61**	**947.609**
CG-4B	**26.446**	**932.229**
CG-5B	**21.828**	**867.567**
CG-1C	**23.511**	**924.788**
CG-2C	**25.702**	**889.276**
CG-3C	**26.608**	**945.155**
CG-4C	**26.394**	**926.902**
CG-5C	**21.825**	**866.606**
CG-1D	**23.52**	**922.995**
CG-2D	**25.794**	**886.395**
CG-3D	**26.772**	**941.098**
CG-4D	**26.586**	**922.794**
CG-5D	**21.91**	**863.558**
CG-1E	**23.517**	**920.054**
CG-2E	**25.9**	**881.331**
CG-3E	**27.101**	**932.826**
CG-4E	**27.129**	**913.384**
CG-5E	**22.303**	**856.71**
CG-1F	**23.521**	**922.956**
CG-2F	**25.796**	**886.341**
CG-3F	**26.775**	**941.027**
CG-4F	**26.589**	**922.725**
CG-5F	**21.911**	**863.508**
Outer bypass	**20.669**	**810.051**